Optics & Laser Technology 140 (2021) 107007

Contents lists available at ScienceDirect

Optics and Laser Technology

journal homepage: www.elsevier.com/locate/optlastec

Full length article

Simplified highly-sensitive gas pressure sensor based on harmonic Vernier effect

Xuemei Yang [a], Shun Wu [a,*], Haihao Cheng [a], Jianwen Ma [a], Shun Wang [a], Shuhui Liu [a], Peixiang Lu [b]

[a] Hubei Key Laboratory of Optical Information and Pattern Recognition, Wuhan Institute of Technology, Wuhan 430205, China
[b] China School of Physics and Wuhan National Laboratory for Optoelectronics, Huazhong University of Science and Technology, Wuhan 430074, China

ARTICLE INFO

Keywords:
Optical fiber sensor
Fabry-Perot interferometer
Highly-sensitive pressure sensor
Vernier effect

ABSTRACT

We propose and demonstrate a simple highly-sensitive gas pressure sensor based on harmonic Vernier effect. By fusion splicing two hollow silica capillaries, a cascaded Fabry-Perot (FP) cavity is formed. Without special photonics crystal fibers or laser machining involved, the fabrication process is greatly simplified. The interplay between the two interferometers consisting the FP cavity leads to optical Vernier effect. By properly adjusting the length of the silica capillaries harmonic of optical Vernier effect is observed and can be served as a sensitive probe for diagnosing gas pressure. Our results showed a sensitivity of 80.8 pm/kPa from 1 to 101 kPa with good linearity of 99.7%, and a low temperature cross sensitivity of 2.22 kPa/°C, a factor of three lower than that of the microstructure fiber-based gas pressure sensors. Combining both ease of fabrication and high sensitivity, this sensor can be a good candidate for mass production in fields of gas sensing and environmental safety monitoring.

1. Introduction

Gas pressure sensing is one of the most important applications of fiber optic devices in industrial and environmental safety monitoring. A variety of optical fiber pressure sensors have been developed based on different mechanism, such as long-period fiber gratings [1–3], anti-resonant waveguide [4,5], and interferometers [6–8]. Considering miniaturization and robustness, high sensitivity gas pressure sensors based on Fabry-Perot Interferometers (FPI) have been extensively studied in recent years. They can be divided into two categories based on the sensing mechanism: either by varying cavity length [9–12], or the refractive index of the sensing cavity due to external pressure [6–8,13,14]. In the former case, a thin flexible diaphragm is usually employed in the FPI design [9,12]. They exhibit high sensitivity up to 39.4 nm/kPa [12]. However, their sensing characteristics depend on the performance of that particular diaphragm. Those sensors usually suffer from limited sensing range, poor linearity and durability.

For FPIs that depend on the variation of refractive index, open cavities have been widely used. The gas inlets are realized by utilizing micro-assembling fibers [13,15],or micro-structured fiber (MSF). In the latter case, micro-machining is usually employed to create lateral holes on MSF by a femtosecond laser or CO_2 laser [14,16,17]. In addition to the fabrication complexity cost, it also demands for superior laser working condition due to the fact that the debris produced usually affects the quality of interference spectra.

An alternative solution to create gas inlet is to use hollow-core silica capillaries. In order to avoid reflection from the end surface, one can use angle cleave [8]. The resulting sensitivity is limited to only a few nm/MPa. An effective way to achieve high sensitivity magnification and improve the sensitivity to tens of nm/MPa is to utilize the Vernier effect [15–19]. In this case, the Vernier condition must be satisfied. That is, the optical path length of the reference cavity has to be close to that of the sensing cavity ($j = 1$), or multiple (j-times, $j > 1$) of it, in addition to a detuning factor. Compared to the fundamental Vernier effect, harmonic Vernier effect [19] is capable of further enhancement of the magnification value with larger fabrication tolerance. Our work explores the fundamental (j = 1) and the first harmonic (j = 2) cases and by applying both in gas pressure sensing. In this paper, we report a simple technique to realize high sensitivity pressure measurement based on cascaded Fabry-Perot cavities using hollow-core silica capillaries. While similar configuration has been reported investigating the fundamental wave [20], our study focuses on exploring the sensitivity magnification generated by the harmonic Vernier effect. Our experimental results the first harmonic showed a highest sensitivity of 80.8 pm/kPa for a

* Corresponding author.
E-mail addresses: wushun_wit@163.com, wushun@wit.edu.cn (S. Wu).

https://doi.org/10.1016/j.optlastec.2021.107007
Received 25 September 2020; Received in revised form 31 January 2021; Accepted 8 February 2021
Available online 24 February 2021

pressure range of 1–101 kPa with excellent linearity, which agreed well with the theoretical simulation based on the interference model. With careful design, one can achieve both high sensitivity and a compact size for the sensor. Moreover, the temperature cross-sensitivity for the sensor was 2.22 kPa/°C, a factor of three lower than that of the microstructure fiber-based gas pressure sensors [18].

2. Sensor principle and fabrication

Fig. 1(a) shows the schematic diagram of the proposed sensor for gas pressure sensing. A Fabry-Perot sensing cavity (denoted by "L_1") was formed by fusion splicing a silica capillary (SC), with length around 333.64 μm and air-core diameter of 75 μm, between a single mode fiber (SMF) and another silica tube, with length about 485.84 μm and hollow-core diameter of 5 μm. Both SCs were purchased from Innosep Scientific Co., Ltd. (Model number: TSP005150). Fig. 1(c) and (d) show the cross-sections of the two SCs. Fig. 1(b) shows the side view image of the sensor head. The 5 μm silica capillary serves both as a reference cavity (denoted by "L_2") and a gas passage that connects the sensing cavity to the external environment. When light propagates from SMF to the air cavity, reflections can occur at three interfaces M1, M2 and M3. This results in three reflection beams, denoted by the red arrows in Fig. 1(a), going back into the SMF. The reflection spectrum is the result of this three-beam interference.

A sensor head can be made by fusion splicing two cascaded silica capillaries to a single mode fiber (SMF). During the fabrication, it is essential to control the cavity length with μms of precision to realize Vernier effect, and also obtain smooth reflection surfaces in the fusion splice. We fabricated four samples S1-S4 with different cavity length configurations, listed in Table 1. All of them satisfy the Vernier condition: $n_{clad}L_2 = jn_{air}L_1 + \Delta L$, where ΔL is the detuning. The cavity lengths were carefully chosen such that the detuning ratio $\Delta L/n_{air}L_1$ for S2-S4 were 16%, 12%, and 9%, respectively (Table 1). S1 has the same detuning ratio with S3 but different *j*. The cavity lengths were calculated based on the measured FSR in the reflection spectrum.

3. Experimental results

Our experimental setup for gas pressure measurement is illustrated in Fig. 2. The proposed pressure sensor was inserted into a vacuum chamber through a steel tube. The connection between the steel tube and the flange was screwed tight to ensure that no gas exchange between the chamber and the external environment. The chamber was evacuated by a mechanical pump. Light from a broadband source (BBS, YSL, 900 nm-1700 nm) went into the sensor through a fiber circulator. The reflection light from the sensor traveled back to the circulator and was measured by the optical spectrum analyzer (OSA, YOKOGAWA AQ6370B) with a maximum resolution of 0.02 nm. A pressure gauge purchased from Cdreborn Electronics Co. Ltd. was used to monitor the gas pressure inside the vacuum chamber, which has a measurement range from 0.5 kPa to 354.7 kPa. Before the measurement, the vacuum chamber was evacuated overnight to remove water vapors inside the chamber and hollow-core capillary until it reached the background pressure of 5×10^{-3} Pa (gauge: KJLC615TC, Kurt J. Lesker). The gas pressure was increased by slowly introducing dry nitrogen gas to the chamber until the chamber reached the desired pressure.

Table 1
Configurations of four different samples.

Sample	L_1(μm)	L_2(μm)	*j*	$\Delta L/n_{air}L_1$
S1	333.64	485.84	2	12%
S2	405.52	323.75	1	16%
S3	309.00	239.50	1	12%
S4	470.55	354.75	1	9%

3.1. Pressure measurement

The pressure measurements of dry nitrogen were taken from 1 kPa to 101 kPa at steps of 10 kPa. The sensing characteristics of all four samples were all investigated. Fig. 3(a) shows the reflection spectrum of S1 under one atmosphere pressure. It exhibited Vernier effect as the high-frequency fringes show periodic envelopes (red curve) in the spectrum. To understand the origin of the interference, we analyzed the correspondent fast Fourier transform (FFT), shown in Fig. 3(b). Four spatial frequency components A, B, C, and D located at 0.3, 0.6,0.9, and 1.2 nm^{-1} correspond to the frequency for cavity L_1, L_2, $(L_1 + L_2)$, and $(2L_1 + L_2)$, respectively. The dominant peaks A and C have most contribution to the measured reflection spectrum. Vernier effect was produced by the superposition of these two interferences. Fig. 3(c) illustrated that the lower envelope near 1517 nm experienced blue shift as pressure increases. The linear fitting showed that the dip of the lower envelope had a sensitivity of −80.8 pm/kPa (black squares) with high linearity of 99.7%, as shown in Fig. 3(d). From Eq. (5) in the Appendix, we can determine the corresponding refractive index of air inside the cavity under a certain pressure. The measured pressure sensitivity is found to be equivalent to a refractive index sensitivity of 30123 nm/RIU for gas sensing. Considering that the OSA has a resolution of 0.02 nm, the accuracy of the pressure sensor is estimated to be about 0.25 kPa.

To investigate the role of *j*, we compared the performances of S1 with other three samples S2, S3 and S4. Fig. 4(a)–(c) showed the reflection spectrum for S2-S4 under one atmosphere. The microscopic side view image of the corresponding sensor was shown in the upper left corner.

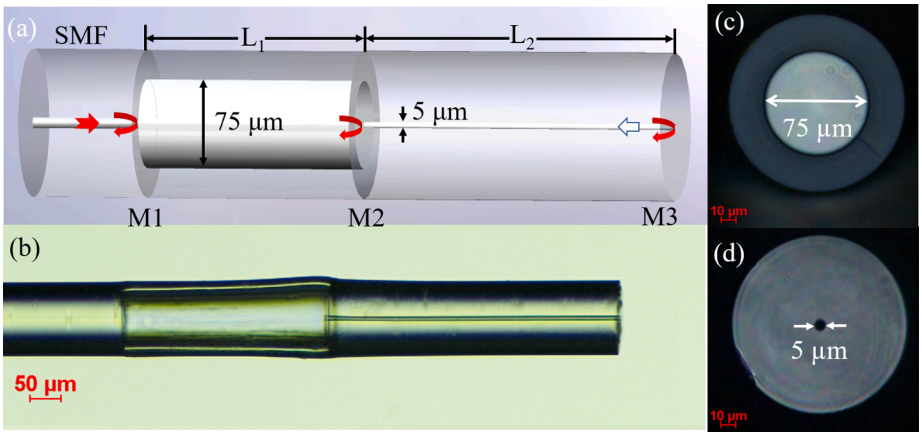

Fig. 1. (a) The schematic diagram of the proposed pressure sensor using silica capillaries. (b) Side-view microscope image of the sensor. Microscope images of the cross section of the silica capillary with air-core diameter of (c) 75 μm and (d) 5 μm.

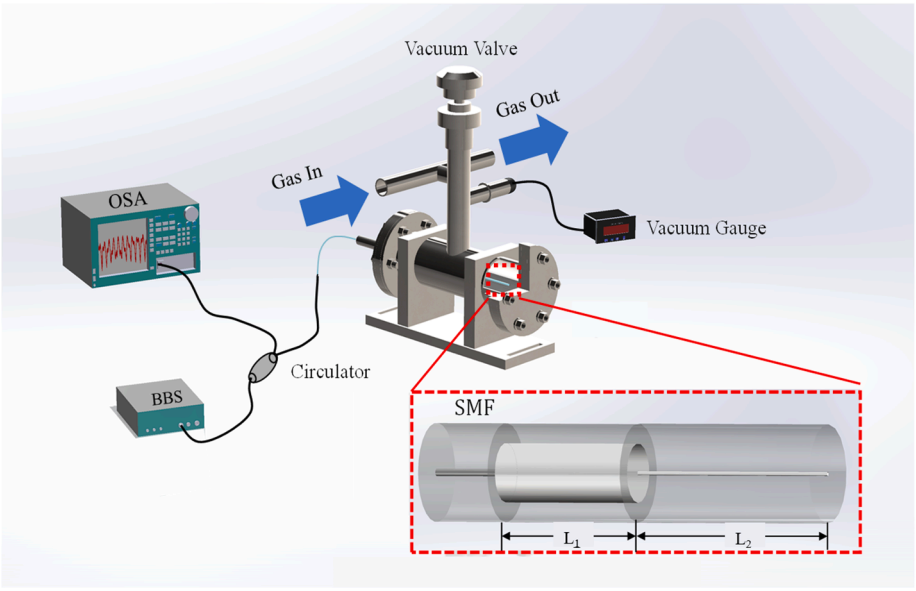

Fig. 2. Experimental apparatus for the gas pressure measurement.

All three sensors exhibited Vernier effect. The measured FSR of envelope are 18 nm, 30 nm and 26 nm, respectively, matching the calculation values based on to Eq. (2) in Appendix. Fig. 4(d) showed the wavelength shifts near 1520 nm for S1-S4 as pressure increased from 1 to 101 kPa. The sensitivity is inverse proportional to the detuning ratio, and proportional to the harmonic order. In the $j = 1$ case, S4 had the smallest detuning ratio of 9%, and thus the highest sensitivity. S1 had similar detuning ratio as S3 but a larger j, the sensitivity of S1 was more than twice of that for S3. The magnification factor is defined as the ratio between the sensitivity of the envelope and the fundamental wave. Table 2 shows that the measured magnification matched well with the calculated values.

3.2. Temperature measurement

Since the refractive index of air in the sensing cavity is dependent on both pressure and temperature, it is important to study the temperature cross-sensitivity for the proposed sensor. We tested the temperature response of S1 by placing it into a column furnace, which has an accuracy of 0.1 °C. Fig. 5(a) showed the shift of the reflection spectrum when the temperature increased from 30°C to 100°C at steps of 10 °C. Each spectrum was recorded after five minutes after the temperature reading became stable. Fig. 5(b) showed that the peak of the lower envelope experienced red shift with increasing temperature. The maximum sensitivity we obtained for various dips near 1520 nm was 179.99 pm/°C with high linearity of above 98.7%. This corresponds to a temperature cross sensitivity of 2.25 kPa/°C, a factor of three lower than the result in [18]. Fig. 5(b) showed that the peak of the lower envelope experienced red shift with increasing temperature, which is the opposite direction as pressure increases. The sign of the magnified sensitivity is determined the sensitivity of a single FP interferometer multiplied by the magnification factor, which in our case is negative due to cavity dimensions (Eq. (3) in Appendix). The pressure sensitivity of a single FP interferometer is calculated to be a positive value (Eq. (5) in Appendix) resulting in a negative magnified sensitivity. However, according to [14], the temperature sensitivity of a single FP interferometer is dominated by the thermo-optic effect with a negative thermo-optic coefficient [14]. Therefore, the magnified sensitivity has a positive value, indicating that the peak of the envelope experiences red shift as temperature increases.

4. Discussion

Based on the above experimental results, the pressure sensitivity is influenced by two factors: the detuning ratio $\Delta L/n_{air}\, L_1$ and the j value, as exhibited in the calculation in Fig. 6(a). The sensitivity has an inverse proportional relationship with the detuning ratio, and linear with j according to Eq. (10) in Appendix. A high sensitivity demands for a small detuning ratio and a large j value. For example, with 4% detuning ratio, the sensitivity can reach 100 pm/kPa even with $j = 1$. This sensitivity is doubled with $j = 2$. However, both factors affect the total sensor length. Fig. 6(b) illustrated how the total sensor length varies as a function of detuning ratio and j, assuming $L_1 = 333$ μm. We can see that as j increases by one, the total length is increased by one sensing cavity length.

Given a limited sensor size, the requirement for a small detuning ratio is equivalent to the precise control for the cavity length. Our current setup with an optical microscope has an uncertainty of about 20 μm for fiber cleave. If we want to reduce the detuning ratio from 12% to 4% for sample S1, we would need a precision within 12 μm. This is difficult to achieve without major modification for the cleaving operation. However, an alternative method to achieve high sensitivity with a moderate precision is to go with a higher j value. The orange dash line in Fig. 6(a) shows that with a detuning ratio of 24%, one can choose a configuration with $j = 4$, and obtain the same high sensitivity, compared to that with a high precision of 6% but $j = 1$.

Suppose one has no constraints for sensor length, there is still an ultimate upper bound for the j value. The major constraint comes from the reduction in the visibility of envelope for higher harmonic orders. According to Ref. [19], the visibility is reduced to be 0.1 dB for the third harmonic ($j = 4$). In our case, a preliminary simulation result shows the visibility may drop to below 0.5 dB for $j = 3$, which is difficult for data analyzation in practical applications. Considering the increased fiber loss for longer cavity lengths, the visibility could be even worse. Several techniques were reported that could improve the visibility of the envelope such as offset splicing [2], however, at the expense of increased transmission loss and the degradation of the mechanical strength of the sensor. Signal processing technique Fast Fourier Transform [3] (FFT) and can be used to remove the high frequency noise in the optical spectrum during the demodulation process. In addition, Ref. [19] introduces a new definition of “internal envelope”, which helps to generate an envelope with moderate visibility for higher order j.

Another constraint is from the dimension of the silica capillary. As

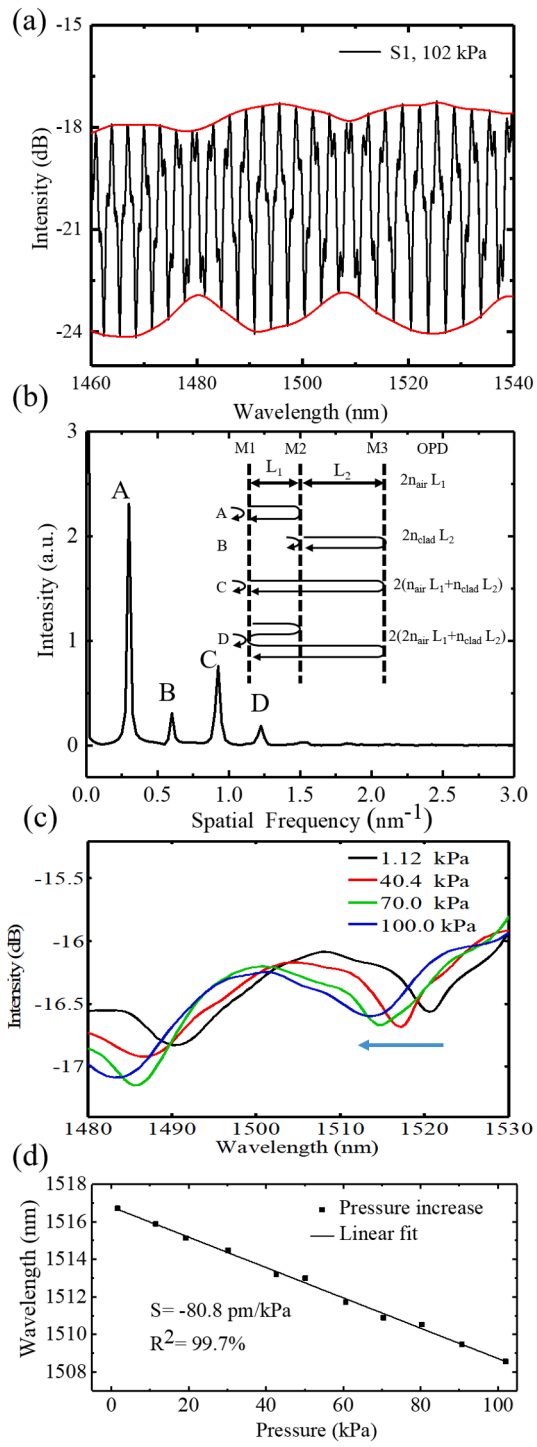

Fig. 3. (a) The spectrum (black fringes) of sensor under pressure 102 kPa and envelope spectrum of the upper and lower edges (red curves). (b) The Fast Fourier Transform (FFT) spectrum for superimposed interference spectrum. (c) The wavelength dip shift about 1520 nm for sensor under different pressure. (d) The linear fitting of different wavelength dip in the pressure change and sensitivity.

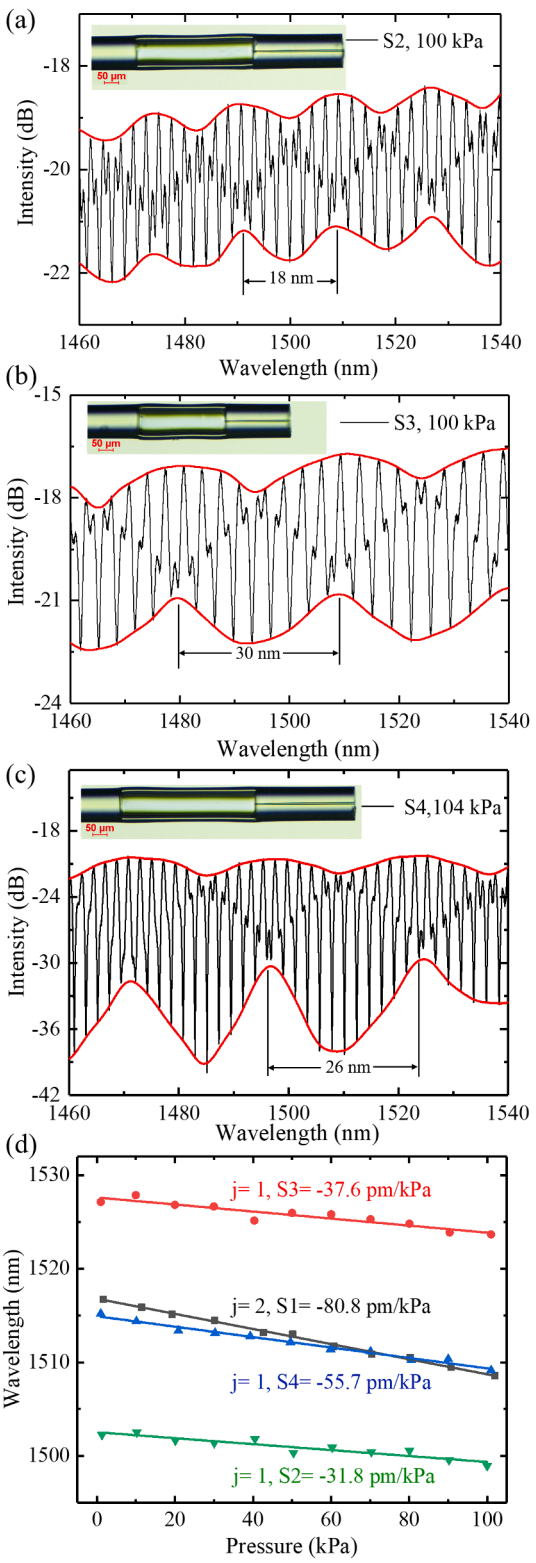

Fig. 4. (a–c) Reflection spectra (black) for samples S2-S4 at 1 atmosphere pressure. The red curves showed the envelopes for Vernier effect. Insets show the microscopic image of the corresponding sensor. (d) Pressure sensitivity comparison near 1520 nm for S1-S4 under 101 kPa.

reported in [21], there exists a critical length of the silica capillary for the onset of the anti-resonant reflecting (AR) effect. Such effect usually does not become appreciable until the capillary reaches a few millimeters long [22]. For the dimensions used in our experiment (few hundred microns long), the AR effect should be trivial. The two-beam approximation [7] model, which ignored the AR effect, can well reproduce the modulation of the experimental spectrum, indicating that the increase in sensitivity is dominated by the utilization of harmonics for the capillary length we used. However, as j is increased, the capillary length may exceed the critical length significantly such that the AR mechanism

Table 2
Comparison of the calculated M-factor with the experimental values.

Sample	M(Cal)	M(Exp)
S1	17.9	18.7
S2	6.3	7.36
S3	8.1	8.7
S4	10.7	12.9

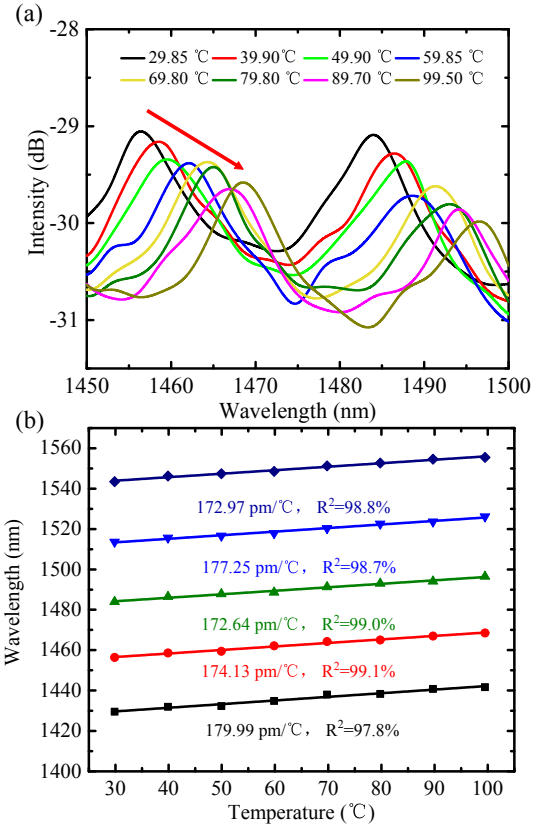

Fig. 5. (a) The wavelength shift of the reflection spectrum for S1 under different temperatures. (b) The temperature sensitivity for various wavelength dips from 1450 nm to 1500 nm.

becomes profound, which can complicate the underlying sensing mechanism.

Regardless the limitations for the *j* value, there are also constraints for the detuning ratio. Since the FSR of envelope FSR_{env} has an inverse proportional relationship with the detuning, reducing the detuning ratio will lead to an increase in the FSR_{env}, which must be within the bandwidth of the transmission window of the sensor. In our case, Vernier effect occurs in the wavelength range from 1400 nm to about 1650 nm, which imposes a constraint for the maximum FSR_{env} to be around 250 nm. When $L_1 = 333$ μm, this corresponds to a detuning ΔL of 4.5 μm. However, if one uses an erbium source with a bandwidth of less than 100 nm, the minimum detuning would be larger than 11 μm.

5. Conclusions

In summary, a compact highly-sensitive pressure sensor based on cascaded Fabry-Perot cavities using simple silica capillaries was experimentally demonstrated in this paper. No complicated fiber machining was involved using high power lasers. Harmonic Vernier effect was demonstrated by precise control of capillary lengths. Our results showed that the pressure sensitivity is inversely proportional to detuning ratio, and proportional to the harmonic order. High sensitivity requires fine-

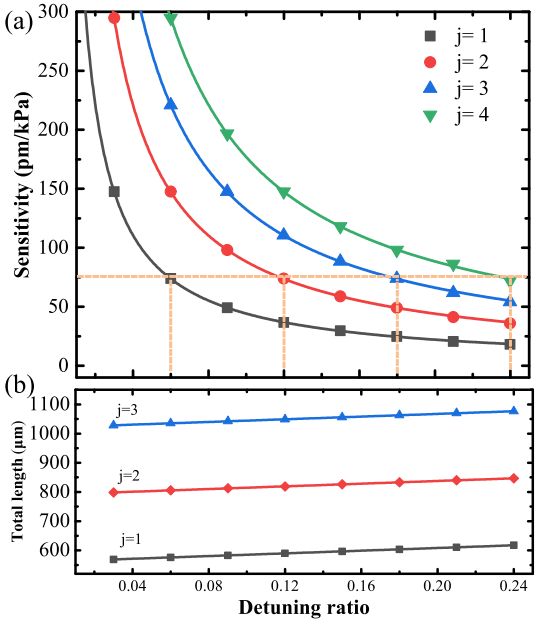

Fig. 6. (a) Pressure sensitivity and (b) Total sensor length as a function of the detuning ratio $\Delta L/n_{air}$ L1 and *j*. Here, the length parameters are: L1 = 333 μm, and ΔL = 37.19 μm.

tuning of the interferometer optical path length, which can be quite technically challenging. Going for higher harmonic orders allows larger tolerances in fabrication without sacrificing sensitivity. With the harmonic order *j* equals to 2, and detuning ratio $\Delta L/(n_{air} L_1)$ of 12%, a high sensitivity of 80.8 pm/kPa was achieved with a linearity of 99.7%. In addition, this sensor had low temperature cross-sensitivity of 2.25 kPa/°C, which was three times lower than cascading cavity design using microstructure fibers [18]. Studies have also shown that silica capillaries can withstand extreme high pressure up to 100 atmosphere [23].

Compared to other reported results using fundamental optical Vernier effect ($j = 1$), our sensor used a simple technique, with combined advantages of high sensitivity and compactness, which made the gas pressure sensor a strong candidate for mass production in gas detection and environmental monitoring fields.

CRediT authorship contribution statement

Xuemei Yang: Conceptualization, Methodology, Software, Formal analysis, Writing - original draft. **Shun Wu:** Data curation, Formal analysis, Writing - original draft, Writing - review & editing. **Haihao Cheng:** Software, Validation. **Jianwen Ma:** Software, Validation. **Shun Wang:** Validation, Writing - review & editing. **Shuhui Liu:** Validation, Writing - review & editing. **Peixiang Lu:** Supervision.

Declaration of Competing Interest

The authors declare that they have no known competing financial interests or personal relationships that could have appeared to influence the work reported in this paper.

Acknowledgments

This work is supported by grants from Natural Science Foundation of China (NSFC) (61805182, 11804258).

Appendix A. Supplementary material

Supplementary data to this article can be found online at https://doi.org/10.1016/j.optlastec.2021.107007.

References

[1] J. Tang, G. Yin, S. Liu, X. Zhong, C. Liao, Z. Li, Q. Wang, J. Zhao, K. Yang, Y. Wang, Gas pressure sensor based on CO_2-laser-induced long-period fiber grating in air-core photonic bandgap fiber, IEEE Photonics J. 7 (5) (2015) 1–7.

[2] X. Zhong, Y. Wang, C. Liao, S. Liu, J. Tang, Q. Wang, Temperature-insensitivity gas pressure sensor based on inflated long period fiber grating inscribed in photonic crystal fiber, Opt. Lett. 40 (8) (2015) 1791–1794.

[3] J. Tang, Z. Zhang, G. Yin, S. Liu, Z. Bai, Z. Li, M. Deng, Y. Wang, C. Liao, J. He, Long period fiber grating inscribed in hollow-core photonic bandgap fiber for gas pressure sensing, IEEE Photonics J. 9 (5) (2017) 1–7.

[4] M. Hou, F. Zhu, Y. Wang, Y. Wang, C. Liao, S. Liu, P. Lu, Antiresonant reflecting guidance mechanism in hollow-core fiber for gas pressure sensing, Opt. Express 24 (24) (2016) 27890–27898.

[5] Y. Yang, D. Wang, B. Xu, Z. Wang, Optical fiber tip interferometer gas pressure sensor based on anti-resonant reflecting guidance mechanism, Opt. Fiber Technol. 42 (2018) 11–17.

[6] R. Wang, X. Qiao, Gas refractometer based on optical fiber extrinsic Fabry—Perot interferometer with open cavity, IEEE Photonics Technol. Lett. 27 (3) (2014) 245–248.

[7] B. Xu, C. Wang, D. Wang, Y. Liu, Y. Li, Fiber-tip gas pressure sensor based on dual capillaries, Opt. Express 23 (18) (2015) 23484–23492.

[8] Z. Zhang, J. He, Q. Dong, Z. Bai, C. Liao, Y. Wang, S. Liu, K. Guo, Y. Wang, Diaphragm-free gas-pressure sensor probe based on hollow-core photonic bandgap fiber, Opt. Lett. 43 (13) (2018) 3017–3020.

[9] J. Ma, W. Jin, H.L. Ho, J.Y. Dai, High-sensitivity fiber-tip pressure sensor with graphene diaphragm, Opt. Lett. 37 (13) (2012) 2493–2495.

[10] F. Xu, D. Ren, X. Shi, C. Li, W. Lu, L. Lu, L. Lu, B. Yu, High-sensitivity Fabry-Perot interferometric pressure sensor based on a nanothick silver diaphragm, Opt. Lett. 37 (2) (2012) 133–135.

[11] C. Liao, S. Liu, L. Xu, C. Wang, Y. Wang, Z. Li, Q. Wang, D. Wang, Sub-micron silica diaphragm-based fiber-tip Fabry-Perot interferometer for pressure measurement, Opt. Lett. 39 (10) (2014) 2827–2830.

[12] Z. Zhang, C. Liao, J. Tang, Z. Bai, K. Guo, M. Hou, J. He, Y. Wang, S. Liu, F. Zhang, High-sensitivity gas-pressure sensor based on fiber-tip PVC diaphragm Fabry-Pérot interferometer, J. Lightwave Technol. 35 (18) (2017) 4067–4071.

[13] M. Deng, C.-P. Tang, T. Zhu, Y.-J. Rao, L.-C. Xu, M. Han, Refractive index measurement using photonic crystal fiber-based Fabry-Perot interferometer, Appl. Opt. 49 (9) (2010) 1593–1598.

[14] Y. Yu, X. Chen, Q. Huang, C. Du, S. Ruan, H. Wei, Enhancing the pressure sensitivity of a Fabry-Perot interferometer using a simplified hollow-core photonic crystal fiber with a microchannel, Appl. Phys. B 120 (3) (2015) 461–467.

[15] M. Quan, J. Tian, Y. Yao, Ultra-high sensitivity Fabry-Perot interferometer gas refractive index fiber sensor based on photonic crystal fiber and Vernier effect, Opt. Lett. 40 (21) (2015) 4891–4894.

[16] H. Lin, F. Liu, H. Guo, A. Zhou, Y. Dai, Ultra-highly sensitive gas pressure sensor based on dual side-hole fiber interferometers with Vernier effect, Opt. Express 26 (22) (2018) 28763–28772.

[17] Z. Li, Y.-X. Zhang, W.-G. Zhang, L.-X. Kong, T.-Y. Yan, P.-C. Geng, B. Wang, High-sensitivity gas pressure Fabry-Perot fiber probe with micro-channel based on Vernier effect, J. Lightwave Technol. 37 (14) (2019) 3444–3451.

[18] P. Chen, Y. Dai, D. Zhang, X. Wen, M. Yang, Cascaded-cavity Fabry-Perot interferometric gas pressure sensor based on Vernier effect, Sensors 18 (11) (2018) 3677.

[19] A. Gomes, M.S. Ferreira, J. Bierlich, J. Kobelke, M. Rothhardt, H. Bartelt, O. Frazão, Optical harmonic Vernier effect: a new tool for high performance interferometric fiber sensors, Sensors 19 (24) (2019) 5431.

[20] H.Y. Liu, Y.Y. Liao, C. Peng, L. Yan, S. Liang, Simple fiber-optic sensor for simultaneous and sensitive measurement of high pressure and high temperature based on the silica capillary tube, Opt. Express 27 (18) (2019) 25777–25788.

[21] Z. Xiaobei, P. Haiyang, B. Huawen, Y. Ming, W. Jiawei, D. Chuanlu, W. Tingyun, Transition of Fabry-Perot and antiresonant mechanisms via a SMF-capillary-SMF structure, Opt. Lett. 43 (10) (2018) 2268–2271.

[22] H. Cheng, S. Wu, Q. Wang, S. Wang, P. Lu, In-line hybrid fiber sensor for curvature and temperature measurement, IEEE Photonics J. 11 (6) (2019) 1–11.

[23] Z. Zhang, J. He, B. Du, F. Zhang, K. Guo, Y. Wang, Measurement of high pressure and high temperature using a dual-cavity Fabry-Perot interferometer created in cascade hollow-core fibers, Opt. Lett. 43 (24) (2018) 6009–6012.